IEICE Proceeding Series

Nonlinear Modal Dynamics in Two-Dimensional Cavity Microlasers

Susumu Shinohara, Takehiro Fukushima, Satoshi Sunada, Takahisa Harayama, Kenichi Arai, Kazuyuki Yoshimura

Vol. 2 pp. 409-412
Publication Date: 2014/03/18
Online ISSN: 2188-5079

2013 International Symposium on Nonlinear Theory and its Applications
NOLTA2013, Santa Fe, USA, September 8-11, 2013

Nonlinear Modal Dynamics in Two-Dimensional Cavity Microlasers

Susumu Shinohara,[†,*] Takehiro Fukushima,[‡] Satoshi Sunada,[§]
Takahisa Harayama,[†,¶] Kenichi Arai,[†] and Kazuyuki Yoshimura[†]

† NTT Communication Science Laboratories, NTT Corporation,
2-4 Hikaridai, Seika-cho, Soraku-gun, Kyoto 619-0237, Japan
‡ Department of Information and Communication Engineering, Okayama
Prefectural University, 111 Kuboki, Soja, Okayama 719-1197, Japan
§ Institute of Science and Engineering, Kanazawa University,
Kakuma-machi, Kanazawa 920-1192, Japan
¶ Department of Mechanical Engineering, Toyo University,
2100 Kujirai, Kawagoe, Saitama 350-8585, Japan
∗ Email: shinohara.susumu@lab.ntt.co.jp

Abstract—We study time-domain properties of outputs from two-dimensional (2D) cavity microlasers theoretically and experimentally. The gain competition of resonant modes is numerically simulated by the Schrödinger-Bloch model that describes nonlinear interaction between the light field and a two-level gain medium. The simulations reveal mode-pulling phenomena that generate beat oscillation of nearby resonant modes and eventually lead to the locking of their frequencies for higher pumpings. Carrying out experiments for semiconductor 2D microlasers, we observe slow modulation of 4-10 MHz in the output signals, which is attributed to the beating of nearly degenerate resonant modes.

1. Introduction

In addition to potential applications in photonics and optoelectronics, two-dimensional (2D) cavity microlasers offer a nice example of complex physical systems where concepts and techniques of nonlinear dynamics and classical/quantum chaos theories play a significant role in understanding observed phenomena [1]. In the last decade, the dependence of lasing emission patterns on 2D cavity shapes has been extensively studied both theoretically and experimentally. In particular, an analogy between optical cavities and quantum billiards has motivated thorough investigations of ray-chaotic cavity microlasers. The manifestation of ray chaos in the (time-averaged) emission patterns of these microlasers has now been well understood. In contrast, less understanding has been obtained for the time-domain properties of 2D microlasers. It is the purpose of this paper to numerically demonstrate a rich variety of nonlinear phenomena in 2D cavity microlasers, and show that they are useful for understanding measured signals output from semiconductor 2D cavity microlasers.

This paper is organized as follows: In Sec. 2, we introduce a theoretical model for 2D microlasers that takes into account nonlinear interaction between the light field and a gain medium. In Sec. 3, we numerically simulate the model, and demonstrate mode-pulling phenomena of nearby resonant modes as well as frequency locking for higher pumpings. In Sec. 4, we report experimental results on 2D cavity semiconductor microlasers that are explained by the interaction of nearly degenerate modes. We close the paper with summary and discussion in Sec. 5.

2. Theoretical model for 2D microlasers

With the assumption that a lasing medium consists of two-level atoms, the light-matter interaction in a 2D microlaser can be described by the Schrödinger-Bloch (SB) model [2]:

$$\frac{\partial \tilde{E}}{\partial t} = \frac{i}{2}\left(\nabla_{xy}^2 + \frac{n^2}{n_{in}^2}\right)\tilde{E} - \alpha\tilde{E} + \mu\tilde{\rho}, \tag{1}$$

$$\frac{\partial \tilde{\rho}}{\partial t} = -(\tilde{\gamma}_\perp + i\Delta_0)\tilde{\rho} + \tilde{\kappa}\, W\tilde{E}, \tag{2}$$

$$\frac{\partial W}{\partial t} = -\tilde{\gamma}_\parallel (W - W_\infty) - 2\tilde{\kappa}(\tilde{E}\tilde{\rho}^* + \tilde{E}^*\tilde{\rho}), \tag{3}$$

where $\tilde{E}(x, y, t)$ and $\tilde{\rho}(x, y, t)$ are the slowly varying envelopes of the TM electric field and of the polarization field, respectively, and $W(x, y, t)$ the population inversion component. In the SB model, the cavity shape determines the spatial distributions of both the refractive index n and the cavity absorption coefficient α. $n(x, y)$ is n_{in}(const) inside the cavity and n_{out}(const) outside the cavity, while $\alpha(x, y)$ is α_L(const) inside the cavity and zero outside the cavity. Space and time are made dimensionless by the scale transformations $(n_{in}\omega_s x/c, n_{in}\omega_s y/c) \to (x, y)$ and $t\omega_s \to t$, respectively, where ω_s is the carrier frequency of the light field slightly different from the transition frequency ω_0 of the two-level medium. The difference of the two frequencies can be measured by a parameter $\Delta_0 = (\omega_0 - \omega_s)/\omega_s$, which plays the role of the gain center. The other parameters are as follows: $\tilde{\gamma}_\perp$ and $\tilde{\gamma}_\parallel$ are the transversal and longitudinal relaxation rates, respectively, μ and $\tilde{\kappa}$ represent the

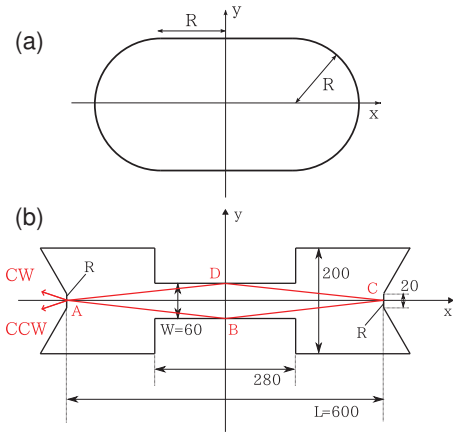

Figure 1: (a) Stadium cavity. (b) Quasi-stadium cavity with a ring orbit connecting A, B, C, and D. The dimensions of the cavity are given in μm. The end mirrors at A and C have a radius of curvature R=320 μm, while the sidewall mirrors at B and D are flat. At the point A, the outputs corresponding to counter-clockwise (CCW) and clockwise (CW) rotating components of the ring orbit are indicated by arrows.

coupling strength between the light field and the medium, and W_∞ is the pumping strength. For the numerical simulations presented here, we fix the cavity shape to be the stadium consisting of two half circles and two flat lines as shown in Fig. 1 (a). The parameter values are set as follows: R=8.662, n_{in}=2, n_{out}=1, Δ_0=−0.075, $\alpha_L=4\times10^{-2}$, $\gamma_\perp=4\times10^{-2}$, $\gamma_\parallel=2\times10^{-2}$, $\tilde{\kappa}$=0.5 and $\mu=\pi/4$.

A key to understanding the dynamics of the SB model is the identification of the resonant modes $\psi_k(x,y)$ ($k=1,2,\ldots$), which are the solutions of the Helmholtz equation

$$-\frac{1}{2}\left(\nabla_{xy}^2+\frac{n^2}{n_{in}^2}\right)\psi_k(x,y)=\xi_k\,\psi_k(x,y). \qquad (4)$$

This eigenequation is obtained by plugging $\tilde{E}=\psi_k(x,y)e^{i\xi_k t}$ into Eq. (1) with $\alpha=\mu=0$ (i.e., an empty cavity). We solve Eq. (4) with the outgoing-wave radiation condition [1], which yields that its eigensolutions, or resonant modes are characterized by complex eigenvalues ξ_k with $\mathrm{Im}\,\xi_k<0$, where $\mathrm{Re}\,\xi_k$ and $\mathrm{Im}\,\xi_k$ respectively represent the oscillation frequency (measured with respect to the gain center) and decay rate of the mode k. We show in Fig. 2 the distribution of complex eigenvalues around $\xi=-0.075$.

Since the stadium cavity has reflection symmetry with respect to both the x- and y-axes, the eigenfunction ψ_k satisfies $\psi_k(-x,y)=a\psi_k(x,y)$ and $\psi_k(x,-y)=b\psi_k(x,y)$ with $a,b=\pm1$. Hence, the eingenmodes are divided into four parity classes labeled by *even-even* (a=b=+1), *even-odd* (a=+1, b=−1), *odd-even* (a=−1, b=+1), and *odd-odd* (a=b=−1). The modes shown in Fig. 2 are labelled accordingly. We show eigenfunctions for the *even-even* and *odd-odd* modes in Figs. 3 (a) and 3 (b).

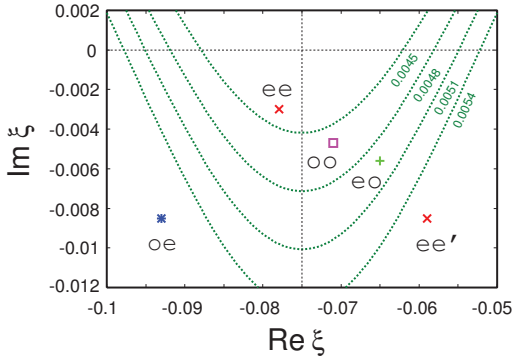

Figure 2: Distribution of eigenvalues ξ of the Helmholtz equation (Eq. (4)) for the stadium cavity. *ee*, *eo*, *oe*, and *oo* represent the parity of a mode. The gain curves $\mathcal{G}(W_\infty)-\alpha_L$ are plotted with dotted curves for W_∞=0.0045, 0.0048, 0.0051, and 0.0054.

3. Nonlinear modal dynamics in 2D microlasers

When the modes are coupled to the lasing medium (i.e., $\mu\neq0$ in Eq. (1)), it supplies energy to the modes, enabling them to lase, that is, Eqs. (1)-(3) start to have stationary lasing solutions for sufficiently large pumping above the lasing threshold. By considering the energy balance between loss and gain, the condition for the mode k to lase is given in the linear limit as

$$\mathcal{G}(W_\infty):=\frac{\mu\tilde{\kappa}\tilde{\gamma}_\perp W_\infty}{\tilde{\gamma}_\perp^2+\left[\mathrm{Re}(\xi_k)-\Delta_0\right]^2}>-\mathrm{Im}(\xi_k)+\alpha_L, \qquad (5)$$

where the left-hand side and the right-hand side represent total gain and total loss, respectively. In Fig. 2 the gain curves (i.e., $\mathcal{G}(W_\infty)-\alpha_L$) for several W_∞-values are plotted. For a given W_∞, the modes above the gain curve are eligible for lasing. As can be seen in Fig. 2, the number of modes with positive net gain increases as the pumping strength W_∞ is increased. The lasing threshold corresponds to the W_∞-value for which the first positive-gain mode (the mode labelled *ee* in the current case) appears. For the parameter values studied here, the lasing threshold is evaluated as $W_\infty\approx0.0045$ from Eq. (5).

We carried out the SB model simulations with increasing the pumping strength W_∞. By analyzing the power spectrum of time series of the electric field, we confirmed single-mode lasing of the mode *ee* for $W_\infty\lesssim0.0050$ (see Fig. 4 (a)), which coincides with the W_∞-regime where only the mode *ee* has a positive net gain. As the pumping is increased further, the second mode *oo* comes into play; for $0.0050\lesssim W_\infty\lesssim0.0078$, we observed two-mode lasing of the modes *ee* and *oo*. We note that for $W_\infty\approx0.0078$, all the five modes shown in Fig. 2 have positive net gain, but most of the energy is sustained by the modes *ee* and *oo*, and the excitation of the other modes is suppressed. The two modes *ee* and *oo* oscillate with different frequencies. A

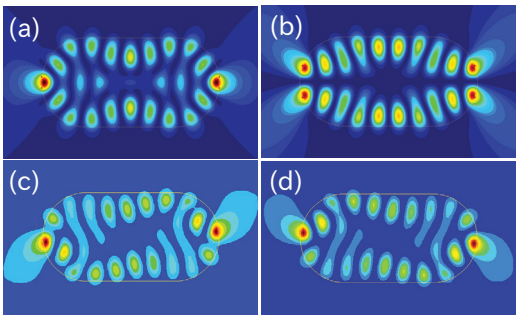

Figure 3: Wave functions for the stadium cavity: (a) *even-even* resonant mode. (b) *odd-odd* resonant mode. (c) and (d) are the snapshots of the light intensity $|\tilde{E}(x,y,t)|^2$ of the SB model for different instants of time (see text).

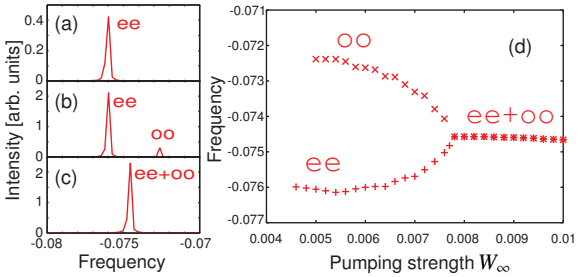

Figure 4: Results of the SB model simulations: Lasing spectra for (a) W_∞=0.0048, (b) W_∞=0.0060, and (c) W_∞=0.0080. (d) The W_∞-dependence of the lasing frequencies of the modes *ee* and *oo*.

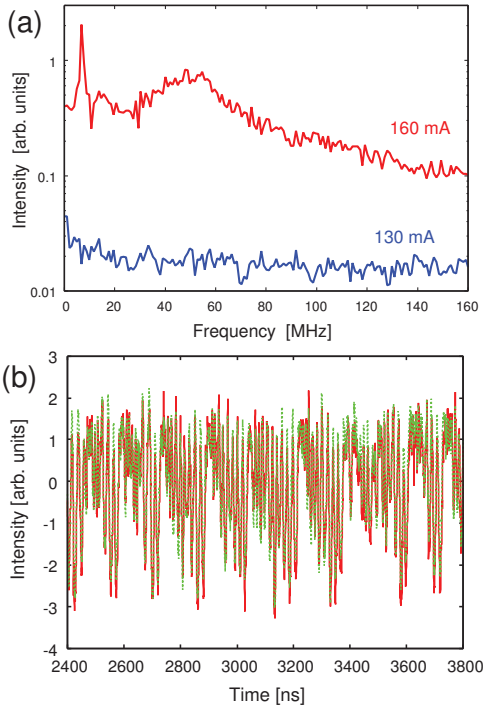

Figure 5: Experimental results for the quasi-stadium cavity semiconductor microlaser: (a) Radio-frequency spectra for the injection currents 160 mA (red) and 130 mA (blue), where the latter gives the noise level. (b) AC-coupled signals for the CCW output (red) and CW output (green) from the quasi-stadium cavity microlaser. Note that the sign of the CW output is reversed in order to see the anti-correlation between the CCW and CW outputs.

typical power spectrum for the two-mode lasing is shown in Fig. 4 (b). The frequency difference becomes smaller as the pumping is increased, and at $W_\infty \approx 0.0078$ they eventually merge, or frequency locking occurs (see Fig. 4 (c)). The W_∞-dependence of the frequencies of the modes *ee* and *oo* is plotted in Fig. 4 (d).

For the single-mode lasing regime (i.e., $0.0045 \lesssim W_\infty \lesssim 0.0050$), the spatial pattern of the light intensity $|\tilde{E}(x,y,t)|^2$ is almost identical to that of the corresponding resonant mode (i.e., Fig. 3 (a)). For the two-mode lasing regime (i.e., $0.0050 \lesssim W_\infty \lesssim 0.0078$), the spatial pattern oscillates with the beat frequency $|\nu_{ee} - \nu_{oo}|$, where ν_{ee} and ν_{oo} are the lasing frequencies of the modes *ee* and *oo*, respectively. When the nonlinearity is small, the light intensity of the lasing state is approximately written as

$$\begin{aligned}\left|\tilde{E}(x,y,t)\right|^2 &\approx \left|\psi_{ee}(x,y)\, e^{i\nu_{ee}t} + \psi_{oo}(x,y)\, e^{i\nu_{oo}t}\right|^2 \\ &= |\psi_{ee}|^2 + |\psi_{oo}|^2 + 2\,\mathrm{Re}\left(\psi_{ee}\psi_{oo}^*\, e^{i(\nu_{ee}-\nu_{oo})t}\right),\end{aligned} \tag{6}$$

where $\psi_{ee}(x,y)$ and $\psi_{oo}(x,y)$ are the eigenfunctions for the modes *ee* and *oo*, respectively. Because of the parity difference between *ee* and *oo*, the third term in the above equation generates an asymmetric spatial pattern as shown in Figs. 3 (c) and 3 (d). The pattern oscillates with the beat frequency $|\nu_{ee} - \nu_{oo}|$. Figs. 3 (c) and 3 (d) are the snapshots of the light intensity $|\tilde{E}(x,y,t)|^2$ for different instants of time separated by the half-period of the beat oscillation. The beat frequency gets smaller as W_∞ is increased (see Fig. 4 (d)), and above the locking threshold $W_c \approx 0.0078$, the spatial pattern of the lasing state is fixed to a static asymmetric pattern.

4. Experiments for quasi-stadium microlasers

Here we report experimental results showing that the modal interaction indeed manifests itself in the output signals from 2D microlasers. We performed experiments for semiconductor microlasers with the quasi-stadium cavity, whose geometry is shown in Fig. 1 (b). The cavity is designed to have the ring modes that are localized along the four-bounce orbit connecting A, B, C, and D (see Fig. 1 (b)). The end mirrors at A and C have a radius of curvature R=320 μm, while the sidewall mirrors at B and D are flat. In the fabrication of the microlasers (see Ref. [3] for details), we patterned the electrode contact along the ring

Table 1: Numerically calculated wavenumbers k for the ring modes of the quasi-stadium cavity with the dimensions given in Fig. 1 (b). Several k-values around $k=2\pi n_{eff}/\lambda$ are given, where λ=0.86 [μm] is the lasing wavelength and n_{eff}=3.3 is the effective refractive index for the semiconductor microlaser.

k [μm^{-1}]	Parity
7.34204	*ee* & *oo*
7.34362	*eo* & *oe*
7.34520	*ee* & *oo*
7.34678	*eo* & *oe*
7.34836	*ee* & *oo*
7.34994	*eo* & *oe*

orbit so that only the ring modes are pumped. Measuring far-field emission patterns, we confirmed the bi-directional output from the ring modes [4]. As shown in Fig. 1 (b), one of the output beams corresponds to the counter-clockwise (CCW) rotating ring orbit, while the other corresponds to the clockwise (CW) rotating ring orbit. Further evidence for the selective excitation of the ring modes is provided by the analysis of measured lasing spectra [4]; we observed multiple peaks with equidistant mode spacing of 0.16 nm. This is in good agreement with the longitudinal mode spacing for the ring modes theoretically estimated as 0.15 nm.

To measure the time-dependence of the bi-directional output, we collect the CCW and CW outputs separately by photodetectors and analyzed them by an oscilloscope. Figure 5 (a) shows a typical radio-frequency (rf) spectrum for the AC-coupled signal for the CCW output. The spectrum exhibits a narrow sharp peak at around 7 MHz as well as a broad peak at around 50 MHz, indicating two different time scales. This can also be confirmed by directly observing the AC-coupled signal of the CCW output $I_{CCW}(t)$, shown in Fig. 5 (b), where we can observe a rapid oscillation corresponding to 50 MHz, together with a slow oscillation corresponding to 7 MHz. Moreover, we can observe anti-correlation between the CCW and CW outputs (i.e., $I_{CCW}(t) \approx -I_{CW}(t)$).

For a wide range of the pumping strengths and irrespective the device, we observed the slow modulation of 4-10 MHz. The slow modulation can be explained by the beating of nearly degenerate modes as below. Because of the cavity's symmetry, each of the ring modes is characterized by the parity *ee*, *eo*, *oe*, or *oo*, in the same manner as in the stadium cavity case. Moreover, it can be shown for the ring modes that either the pair *ee* and *oo* or the pair *eo* and *oe* constitutes a nearly degenerate pair [5]. Table 1 shows the wavenumbers of the ring modes calculated numerically, where we can confirm the above pairing rule as well as the longitudinal mode spacing of $\Delta k \approx 0.00158$ [μm^{-1}]. The wavenumber difference between a nearly degenerate pair is too small to be detected in our numerical calculations because of the accuracy limitations. According to the SB simulations discussed in Sec. 3, such nearly degenerate pairs are expected to strongly interact, thereby generating slow beat oscillations. Therefore, we can interpret the observed slow modulation as the manifestation of the near degeneracy. By denoting the wavenumber difference as Δk, the beat frequency is written as $\Delta\nu = c\Delta k/(2\pi)$, which yields that the slow modulation of 7 MHz can be explained by the wavenumber difference $\Delta k \approx 1.5 \times 10^{-7} \mu m^{-1}$.

5. Summary and Discussion

Numerically simulating the nonlinear lasing dynamics of the 2D microlaser, we demonstrated the beating of nearby modes and their frequency locking. In addition, we reported experimental results on the robust observation of slow modulation in the output signals from semiconductor 2D microlasers, and explained them by the beating of nearly degenerate resonant modes. In our experiments, we could not observe the tendency toward the frequency locking even for higher pumpings. We consider this is due to a large locking threshold. In fact, the threshold could be very large in the SB model simulations depending on the choice of parameter values and the distribution of modes' eigenvalues. Another significant difference between the simulations and experiments is that only a single nearly degenerate pair is excited in the simulations, while multiple (more than 10 for the data presented in Fig. 5) pairs are excited in the experiments. Our observation of the sharp peak in the rf spectrum indicates that the excitation of the multiple nearly degenerate pairs occur coherently. The mechanism achieving this coherency will be reported elsewhere.

References

[1] T. Harayama and S. Shinohara, "Two-dimensional microcavity lasers," *Laser Photonics Rev.* vol. 5, pp. 247-271, 2011.

[2] T. Harayama, S. Sunada, and K. S. Ikeda, "Theory of two-dimensional microcavity lasers," *Phys. Rev. A*, vol. 72, p. 013803, 2005.

[3] T. Fukushima and T. Harayama, "Stadium and quasi-stadium laser diodes," *IEEE J. Sel. Top. Quant. Electron.*, vol. 10, pp. 1039-1051, 2004.

[4] S. Shinohara, T. Fukushima, S. Sunada, T. Harayama, K. Arai, and K. Yoshimura, "Anti-correlated bi-directional output from quasistadium-shaped microlasers," *submitted*.

[5] H. E. Tureci, H. G. L. Schwefel, A. D. Stone, and E. E. Narimanov, "Gaussian-optical approach to stable periodic orbit resonances of partially chaotic dielectric micro-cavities," *Opt. Express*, vol. 10, pp. 752-776, 2002.